Journal of Membrane Science 636 (2021) 119286

Contents lists available at ScienceDirect

Journal of Membrane Science

journal homepage: www.elsevier.com/locate/memsci

Electroconvective circulating flows by asymmetric Coulombic force distribution in multiscale porous membrane

Dokeun Lee [a], Daehyun Choi [b], Hyungmin Park [b,c], Hyomin Lee [d,**], Sung Jae Kim [a,e,f,*]

[a] Department of Electrical and Computer Engineering, Seoul National University, Seoul, 08826, Republic of Korea
[b] Department of Mechanical and Aerospace Engineering, Seoul National University, 1 Gwanak-ro, Gwanak-gu, Seoul, 08826, Republic of Korea
[c] Institute of Advanced Machines and Design, Seoul National University, 1 Gwanak-ro, Gwanak-gu, Seoul, 08826, Republic of Korea
[d] Department of Chemical and Biological Engineering, Jeju National University, Jeju, 63243, Republic of Korea
[e] Inter-university Semiconductor Research Center, Seoul National University, Seoul, 08826, South Korea
[f] Nano Systems Institute, Seoul National University, Seoul, 08826, South Korea

ARTICLE INFO

Keywords:
Concentration polarization
Electroconvection
Circulating flow
Permselective membrane
Overlimiting current

ABSTRACT

Electroconvection (EC) near an ion-selective membrane has attracted significant attention in concentration polarization platform and been generally accepted as a cause of the overlimiting current. Especially, the heterogeneous structures of the ion-selective membrane have been extensively studied for enhancing perm-selective mass transportations in an EC-dominant regime. However, there is lack of studies considering EC on a multiscale porous membrane, which has been often utilized in desalination and fuel cell platform. In this work, we developed a modeled micro/nanofluidic device consisted of an array of ion-selective patches so that micropores were formed between the patches. Rigorous theoretical and experimental analysis on EC near the membrane demonstrated that asymmetric Coulombic force distribution among the micropores induced electroconvective circulating flows, leading to significant enhancement of ion transport and lowering resistivity of the entire system. Furthermore, we verified that the appearance of the circulating flow critically depended on the configuration of micropores so that one can maximize the ion transportation by tweaking the configuration. Therefore, the new finding of the circulating flows would advance the fundamental understanding of electrokinetics in concentration polarization platforms which have been extensively applied for environmental and energy applications.

1. Introduction

Electroconvection (EC) in the electrolyte near an ion-selective membrane has gained great attention in a concentration polarization platform that induces significant concentration gradient at both sides of the membrane under a sufficiently strong dc electric field [1–10]. It has been reported that ion transport is saturated to a limiting current, if one considered only classical diffusion-drift theory since the concentration at the surface of an ion-selective membrane approaches zero [11]. However, when the voltage increases beyond a threshold value, the experimentally observed strong vortices induced by EC supply additional ionic flux to the membrane, so that the ionic current increases above the saturated value (limiting current), which is called the overlimiting current [12–19]. The fundamental studies on EC are important in order to analyze the overlimiting current regime since various applications such as electrodialysis (ED) [20–28], electrodeionization (EDI) [29–32], sample separation/preconcentration [33–38], and fuel cell [39] need to have enhanced ionic mass transport at their high operation voltage. Recent studies suggested that the extended space charge layer (ESCL) over an electrical double layer (EDL) adjacent to the membrane becomes gradually unstable due to positive feedback by small perturbations under a sufficiently high electric field in the case of conventional homogeneous membrane (Fig. 1(a)-(i)) [15,40–43]. The fluctuation of the ESCL induces tangential electric fields ($E_{||}$) along the membrane (Fig. 1(a)-(ii)), leading to Coulombic force-driven fluid motions called the second-kind electroosmotic flow (*i.e.* nonequilibrium electroconvective instability, Fig. 1(a)-(iii)) [40,44–46]. However, a number of practical systems have utilized the membrane of multiscale

* Corresponding author. Department of Electrical and Computer Engineering, Seoul National University, Seoul, 08826, Republic of Korea.
** Corresponding author. Department of Chemical and Biological Engineering, Jeju National University, Jeju, 63243, Republic of Korea.
E-mail addresses: fluid@jejunu.ac.kr (H. Lee), gates@snu.ac.kr (S.J. Kim).

https://doi.org/10.1016/j.memsci.2021.119286
Received 27 January 2021; Received in revised form 8 March 2021; Accepted 14 March 2021
Available online 29 March 2021

pores such as micropores between ion-selective granules in EDI system [47–51], a multiscale-porous ion selective membrane in ion concentration polarization system [52–54] and poly-dispersed micro/-nanostructures in concentration polarization system [55], *etc*. These studies commonly reported that the multiscale porous membrane enabled to enhance a mass transport by suppressing the growth of an ion depletion zone or adding supplementary ionic current paths.

In the meantime, our group extensively studied the effect of non-negligible water permeance through a nanoporous membrane [56,57]. Small but critical water permeance significantly increased the over-limiting current due to the suppression of instability by normal flow to the membrane and affected ion concentration profiles near the membrane [58,59]. To resemble a practical platform where a normal flow through the membrane is critical factor, in this work, we presented the systematic multiscale porous membrane system. The modeled system was rigorously analyzed and we found a new type of electroconvective circulating flow that were unable to be explained by conventional instability theory.

Precisely modeled patch structures of ion-selective membrane through which fluid could flow were considered in this study by theoretical and experimental manner. In the diagram shown in Fig. 1(b), symmetric Coulombic force was generated among the micropores in Ohmic/limiting regime. However, when the electric field became sufficiently high (*i.e*. in overlimiting regime), the initial fluctuation of ESCL (Fig. 1(b)–(i)) led to asymmetric (unstable) EC (Fig. 1(b)-(ii)), which randomly distributed the charges inside ESCL among micropores. Therefore, interestingly, ESCL in several micropores was overlapped, while one in others was not overlapped, leading to a significant asymmetric Coulombic force distribution (Fig. 1(b)-(iii)). The asymmetry among the micropores triggered electroconvective circulating flows for satisfying a continuity condition (Fig. 1(b)-(iv)). This is the mechanism of the electroconvective circulating flow, even in the domain where all the patches and distances were perfectly symmetric. In this work, the circulating flows were investigated based on numerical simulations of Poisson-Nernst-Planck and Stokes equations in a 2D domain, and *in situ* visualizations/measurements, which unveiled a new electrokinetic phenomenon near a multiscale porous membrane. Moreover, we demonstrated the impact of periodicity of the patches on current density, which can provide a practical design rule for a system that requires highly efficient mass transport.

2. Methods

2.1. Numerical methods

We considered a symmetric binary electrolyte such as KCl solution filled in a rectangular domain which included periodic ion-selective patches in the middle. As shown in Fig. 2(a), the height of the domain and cation-selective patch is 2.5 and 0.5, respectively and the width of micropores and cation-selective patches was identical as *w*. This multiscale membrane allowed the fluid to pass through the micropores, while only cations can pass through the patches. Thus, our system simply, but robustly modeled one side of EDI platform [48–51](*i.e*. cation-selective patches in a bulk) and a recently reported nanofluidic preconcentrator, which is useful in a micro-total-analysis system [52,54].

Here, the dimensionless Poisson equation, Nernst-Planck equations, mass conservation and incompressible Stokes equations described electric potential, ion transport and flow, respectively as

$$-\nabla^2\varphi = \rho_e = \frac{1}{2\lambda_D^2}(c_+ - c_-) \tag{1}$$

$$\frac{\partial c_\pm}{\partial t} = -\nabla\cdot\mathbf{j}_\pm = -\nabla\cdot[-\nabla c_\pm \mp c_\pm\nabla\varphi + c_\pm\mathbf{u}], \tag{2}$$

$$\nabla\cdot\mathbf{u} = 0 \text{ and} \tag{3}$$

$$\frac{1}{Sc}\frac{\partial\mathbf{u}}{\partial t} = -\nabla p + \nabla^2\mathbf{u} - \frac{\kappa}{2\lambda_D^2}(c_+ - c_-)\nabla\varphi \tag{4}$$

in electrolyte. Due to impermeability, they were reduced as

$$-\nabla^2\varphi = \rho_e = \frac{1}{2\lambda_D^2}(c_+ - c_- - N) \text{ and} \tag{5}$$

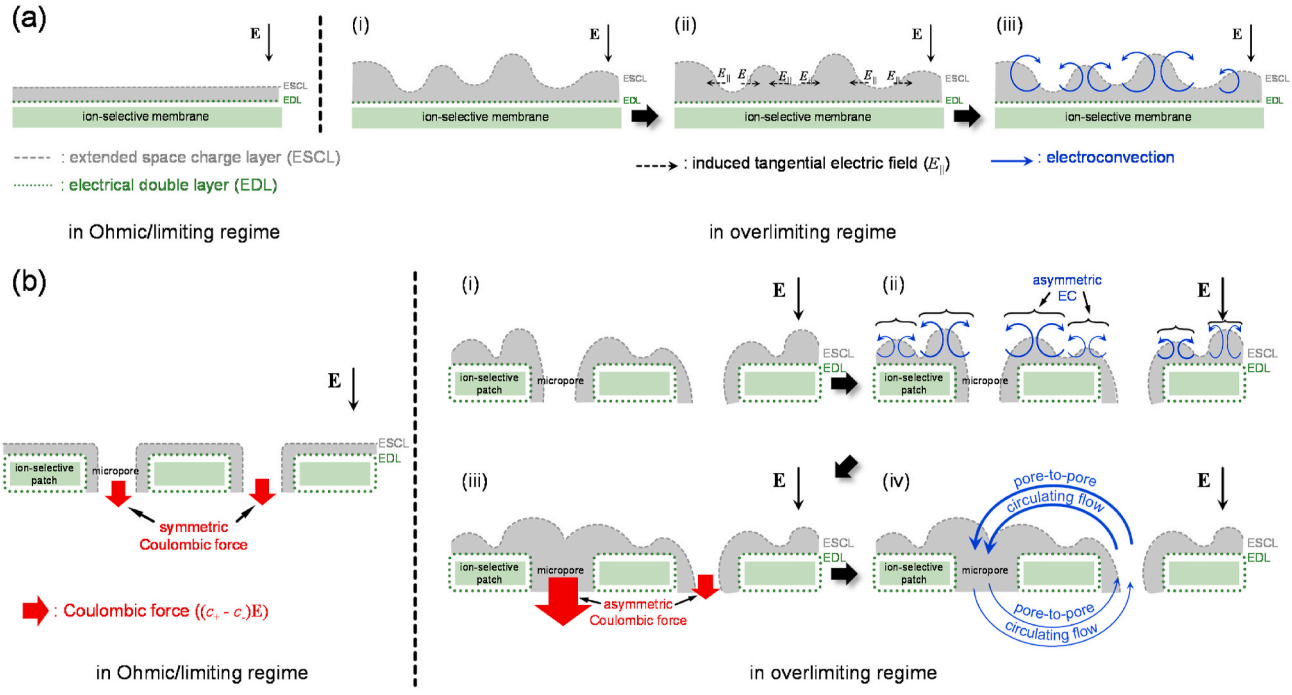

Fig. 1. Schematic diagrams for illustrating the mechanism of (a) electroconvective vortices in a conventional (flat) ion-selective membrane and (b) electroconvective circulating flows near multiscale porous membrane.

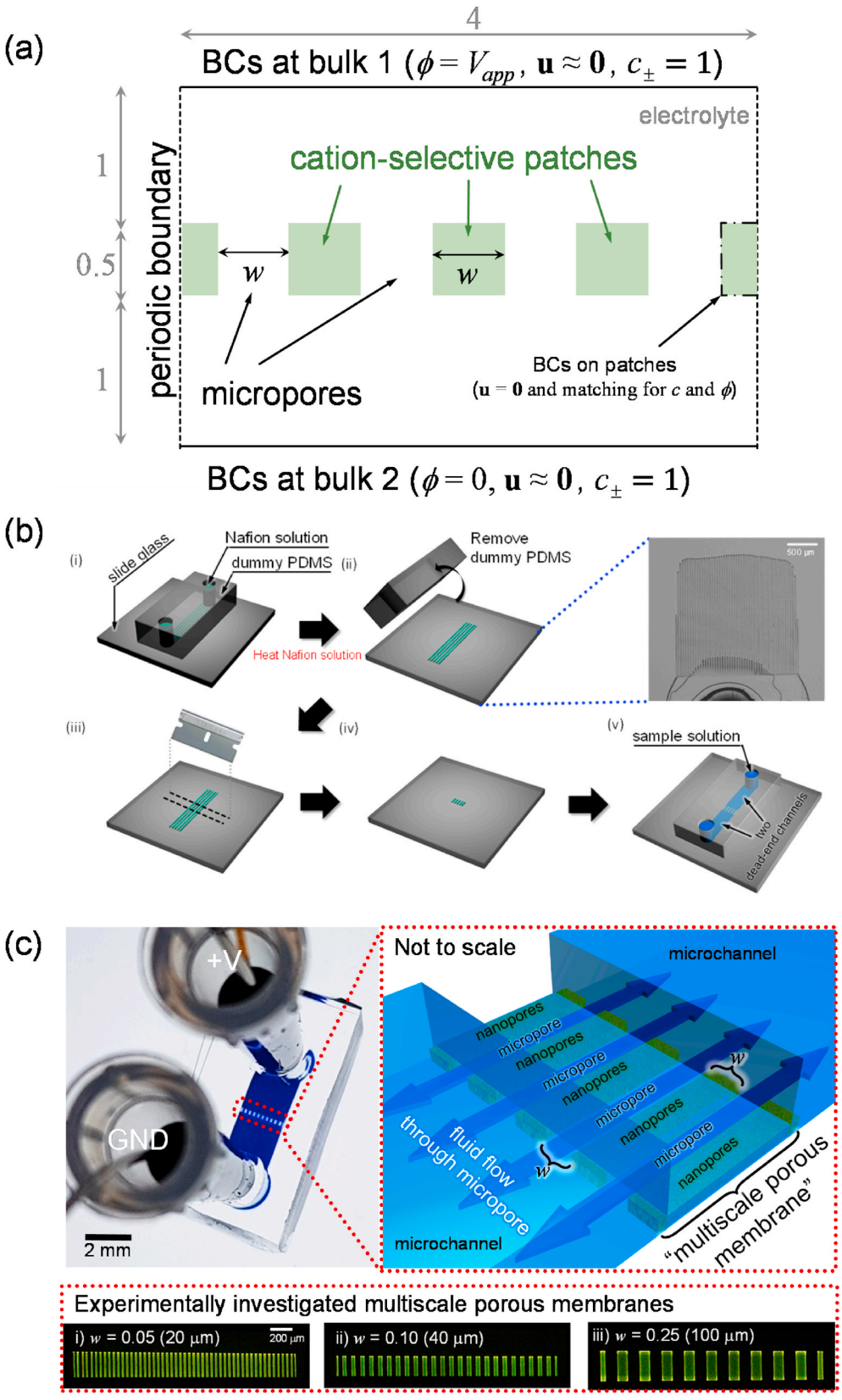

Fig. 2. (a) The schematic diagram of numerical domain for multiscale porous membrane. (b) Fabrication process of micro/nanofluidic device with multiscale porous membrane. (c) Image of fabricated micro/nanofluidic device with schematics of flows through micropores.

$$\frac{\partial c_{\pm}}{\partial t} = -\nabla\cdot\mathbf{j}_{\pm} = -\nabla\cdot[-\nabla c_{\pm} \mp c_{\pm}\nabla\varphi] \quad (6)$$

inside cation-selective patches. In the above equations, φ was the applied dc voltage across the domain vertically, ρ_e was the free charge density, λ_D was the Debye length, c_+ and c_- were the concentrations of cations and anions, t was the time, $\mathbf{j}_{\pm}$ were the ion fluxes of cations and anions, $\mathbf{u}$ was the velocity, Sc was the Schmidt number which is the ratio of viscous diffusion rate to mass diffusion rate, p was the pressure, κ was the electrohydrodynamic coupling constant as $\kappa = \frac{\varepsilon V_T^2}{\mu D}$ where V_T is k_BT/ze and N was the fixed charge concentration of the cation-selective patches (*i.e.* Donnan concentration) [42]. All quantities were non-dimensionalized by distance from the patches to the stationary bulk, thermal voltage, bulk concentration, diffusion velocity, and diffusion time. Dimensionless boundary conditions at bulk1 and bulk2 were given as $c_{\pm} = 1$, $\mathbf{u} \approx \mathbf{0}$, and $\varphi = V_{app}$ (bulk1), and $\varphi = 0$ (bulk2). Periodic boundary conditions were applied across the domain laterally. The boundary conditions on the cation-selective patches were no-slip condition for flow field and matching condition for electric potential and electrolyte concentration (*i.e.* $\partial\varphi_{patch}/\partial\mathbf{n} = \partial\varphi_{electrolyte}/\partial\mathbf{n}$ and $\partial c_{patch}/\partial\mathbf{n} = \partial c_{electrolyte}/\partial\mathbf{n}$), which are not specific conditions for electroosmotic flow (EOF) or induced charge electroosmotic flow (ICEO), but the general boundary condition. N of the patch was set as 100 which was much higher than $c_{\pm}$ and the positive number for representing cation-selectivity. For typical aqueous 1 mM electrolyte, κ, λ_D, and Sc were set as 0.5, 0.001, and 1000, respectively, because it has been reported that κ is typically close to 0.5 for aqueous solution and there is not wide range of choice on this parameter [41,42,60]. All of governing equations and boundary conditions were solved by commercial FEM software (general form PDE, Poisson's equation and creeping flow modules in COMSOL Multiphysics). For appropriate numerical process, a non-uniform mesh structure was introduced after proper convergence test. See the details in supporting information.

2.2. Experimental methods

To experimentally investigate the electrokinetics in the domain, a micro/nanofluidic chip was designed as shown in Fig. 2(b). The micro/nanofluidic chip consisted of cation-selective membrane (Nafion, Sigma Aldrich, USA) patterned on a glass slide and polydimethyl-siloxane (PDMS, Sylgard 184 silicone elastomer kit, Dow Corning, USA) block having two dead-end microchannels. Brief fabrication processes were as follows. As shown in Fig. 2(b), (i) A dummy PDMS block of a straight microchannel (depth 40 μm × length 4 mm × width 2 mm) that had multiple fin structures was reversibly bonded on top of a slide glass. Nafion solution was injected into the straight microchannel. The fin had the dimension of depth 40 μm × length 4 mm × width 20 μm, 40 μm, or 100 μm, respectively, and the spacing between fins was the same with the width in a device. Thus, there were 50, 25 and 10 fins inside the straight microchannel. (ii) After heating 95 °C for 10 min, the dummy PDMS block was removed to leave long Nafion strips on top of the glass slide. See the microscopic image. The thickness of Nafion strip was 20 μm. (iii-iv) Using razor cut twice under an observation by microscope, multiple Nafion patches of 250 μm length were carved. (v) The PDMS block of the two dead-end microchannels and Nafion patterned slide glass were irreversibly bonded using oxygen plasma treatment (CuteMP, Femto Science, Korea). The two dead-end microchannels had the dimension of depth 150 μm × length 2 mm × width 2 mm and were 200 μm apart. Then, multiple micropores (depth 20 μm × length 200 μm × width 20, 40 or 100 μm) between Nafion patches connected the two dead-end microchannels as shown in Fig. 2(c). Nafion patches were periodically patterned depending on w. The thickness of patterned Nafion patches was 20 μm so that the fluid can pass only through the micropores between Nafion patches. Dimensionless ws of 0.05, 0.10 and 0.25 corresponded to 20 μm, 40 μm and 100 μm, respectively. If the width is larger than 100 μm, the micropores would collapse, impeding or blocking fluid flows [61]. For the visualization of the concentration profiles and flow streamlines, Alexa Fluor 488 (Invitrogen, USA) and negatively charged 1 μm particles (Invitrogen, USA) in 1 mM KCl solution (Sigma Aldrich, USA) were used. The concentration profiles and the motions of charged particles were imaged using an inverted fluorescence microscope (IX53, Olympus, Japan) and CellSens (Olympus, Japan) program. An external voltage ($\widetilde{V}_{app}$) was applied using a source measure unit (Keithely 236, USA) via Ag/AgCl electrodes inserted into two reservoirs. Note that the dimensionless electric field ($\widetilde{E}$) is defined as ($\widetilde{V}_{app}/V_{th}$)/(8.2 mm/0.2 mm) in experiment and V_{app}/(2.5/0.5) in simulation where V_{th} is the thermal voltage. Residual pressure by unwanted level difference of liquid in reservoir was regulated by a syringe pump (PHD2000, Harvard Apparatus, USA).

3. Results and discussions

3.1. Verification of electroconvective circulating flow

Fig. 3 shows the electrolyte concentration profiles associated with the electroconvective circulating flows which were generated near the multiscale porous membrane. In the case of conventional flat membrane (*i.e.* without micropores), an ion depletion zone (IDZ) and an ion enrichment zone (IEZ) were formed at the anodic and cathodic side of the membrane, respectively. However, abundant ions of IEZs were pumped up to the anodic side through micropores near center in the case of the multiscale porous membrane as shown in Fig. 3(a) (simulation) and 3(b) (experiment), which indicated that a portion of ions in IEZ came up to form a circulated IEZ (cIEZ) above the membrane. In the meantime, IDZs were pumped down to cathodic side through left and right micropores to form a circulated IDZ (cIDZ) under the membrane. See Supplementary Video 1. The direction of this circulation was in line with the streamline shown in Fig. 3(c) (simulation). It was upward in the middle and downward at both sides of the membrane. Because the electric field inside IDZ significantly amplified, the speed of circulation above the membrane would be much faster than one under the membrane. The directions and speeds were experimentally verified as shown in Fig. 3(d). Since negatively charged particles were used as tracers of fluid flows, they were rejected to enter IDZs formed inside micropores (*i.e.* right and left side of the membrane) [6], hindering exact visualization of the circulating flows. Instead, the tracers moved upward through the micropores in the middle as shown in the flow streamline of Fig. 3(d) using particle image velocimetry (PIV) analysis (see cyan solid line). Note that the tracers in the region above the membrane moved extremely fast and, thus, PIV analysis was applied to only under the membrane. Cyan broken lines above the membrane are artificial. Nonetheless, it indirectly proved the existence of electroconvective circulating flows. See Supplementary Video 2. Moreover, as shown in Fig. 3(e), the formations of the circulating flow were completely different in each trial even they were conducted with the same device, since the mechanism behind the circulating flow was the electroconvective instability. See Supplementary Video 3. At the same time, we can derive the distortion of ESCL as shown in Fig. 4. One can calculate the magnitude of Coulombic force ($|\mathbf{F_c}|$) as $\left|\int_w (c_+ - c_-)\mathbf{E}dl\right|$ and the distributions along the membrane were shown in the bar plot. As expected, $\mathbf{F_c}$ was stronger at the sides than one in the middle in the case of $w = 0.25$ (the third column) so that this relative difference induced the electroconvective circulating flow (indicated with thick blue arrows) near the membrane to satisfy a continuity condition. While similar scenarios were applied to various w values, slight difference resulted in weak circulating flows in the case with narrower ($w = 0.05$) or wider (w = 0.5 and 1) micropores. Note that vortices on the membrane were conventional electroconvective flows.

Supplementary video related to this article can be found at https://doi.org/10.1016/j.memsci.2021.119286.

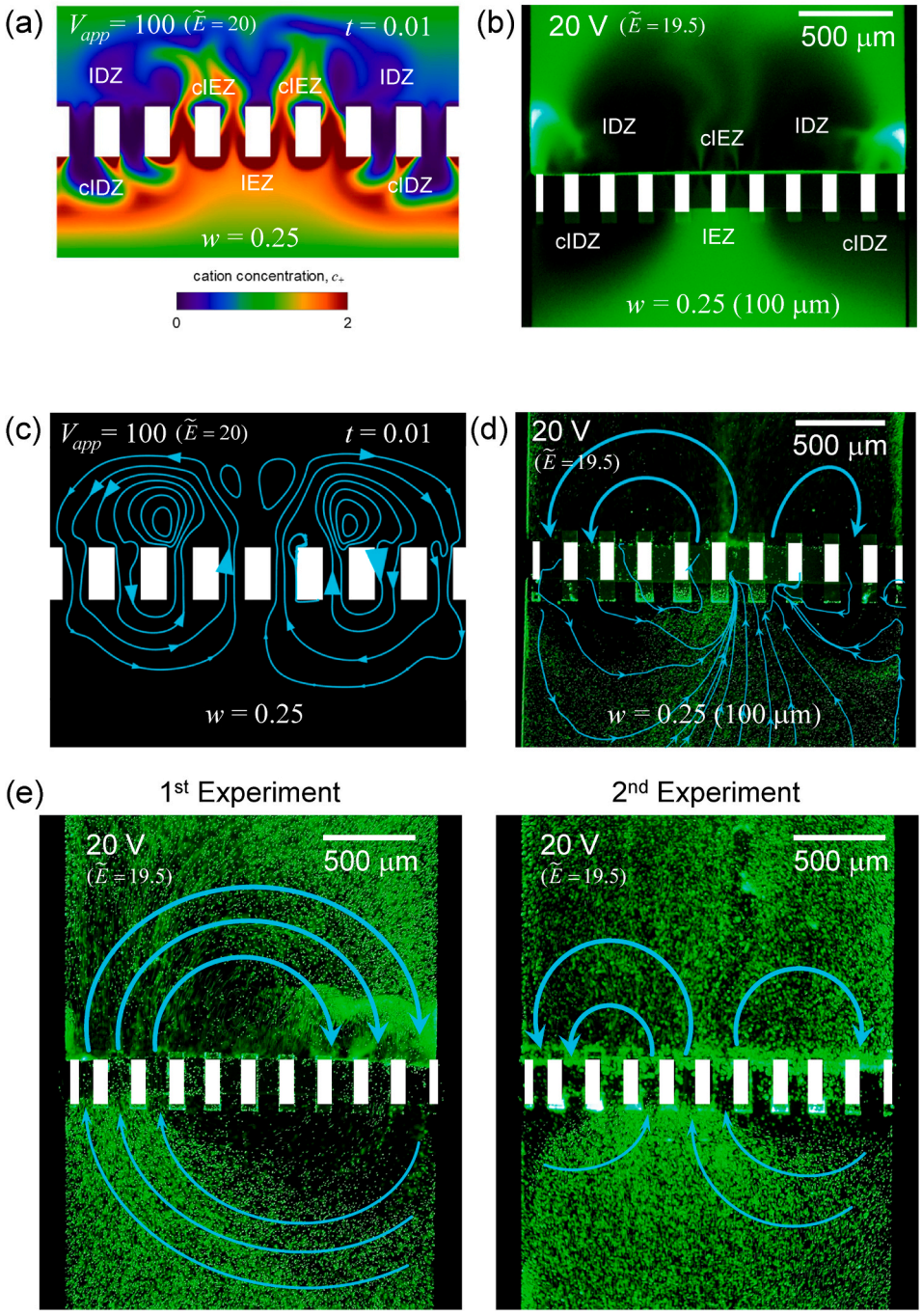

Fig. 3. (a) Numerically simulated concentration profiles under $V_{app} = 100$ ($\tilde{E} = 20$) at $t = 0.01$ and (b) experimentally obtained concentration profiles under 20 V ($\tilde{E} = 19.5$) using a fluorescent dye. IDZ and IEZ denoted the ion depletion zone and the ion enrichment zone respectively. Prefix "c" meant "circulated". (c) Numerically simulated flow streamlines under $V_{app} = 100$ ($\tilde{E} = 20$) at $t = 0.01$ and (d) experimentally obtained flow streamlines under 20 V ($\tilde{E} = 19.5$) using PIV analysis. All cases were examined with $w = 0.25$. (e) While these images were taken at the identical conditions and the device, the formations of EC circulating flow were completely different in each trial due to the instability.

3.2. Space charge overlap depending on w

The formation of cIEZ associated with the circulating flows critically reduced the electrical resistance of the entire system so that the appearance of circulating flows was closely related to the ion transportation through the multiscale porous membrane system. Here we present a case study about the effect of the distance between the patches. By maintaining the width of the patch and the micropore at 1:1 ratio, *w*s in simulation were selected as 0.05, 0.1, 0.25, 0.5 and 1 as shown in Fig. 4. When the patch size was large ($w = 0.5$ or 1 (the fourth and fifth column of Fig. 4)), ESCLs induced by asymmetric EC were non-overlapped inside all micropores. Accordingly, $|\mathbf{F_c}|$s in all micropores had almost the same values as shown in the bar graphs. Thus, the circulating flows were merely generated due to symmetric $\mathbf{F_c}$. On the other hand, ICEO could be the factor to induce the intrapore vortices in the case of large *w*, if there is no or weak surface charge [62]. However, the presenting system has the multiscale porous membrane with high surface charge; in simulation, we chose Donnan concentration (*N*) as 100 which is higher than bulk concentration ($c_\pm = 1$) and in experiment, we used Nafion and PDMS which have high surface charge [63]. Therefore, the surface charge is predominantly high so that electroconvection due to extended space charge overwhelms ICEO vortices. However, as the patch size decreased ($w = 0.1$ and 0.25 (the second and third column of Fig. 4)), ESCLs were asymmetrically distributed due to unstable EC, which resulted in the significant difference of $|\mathbf{F_c}|$s inside micropores as shown in the bar graphs. Therefore, the electroconvective

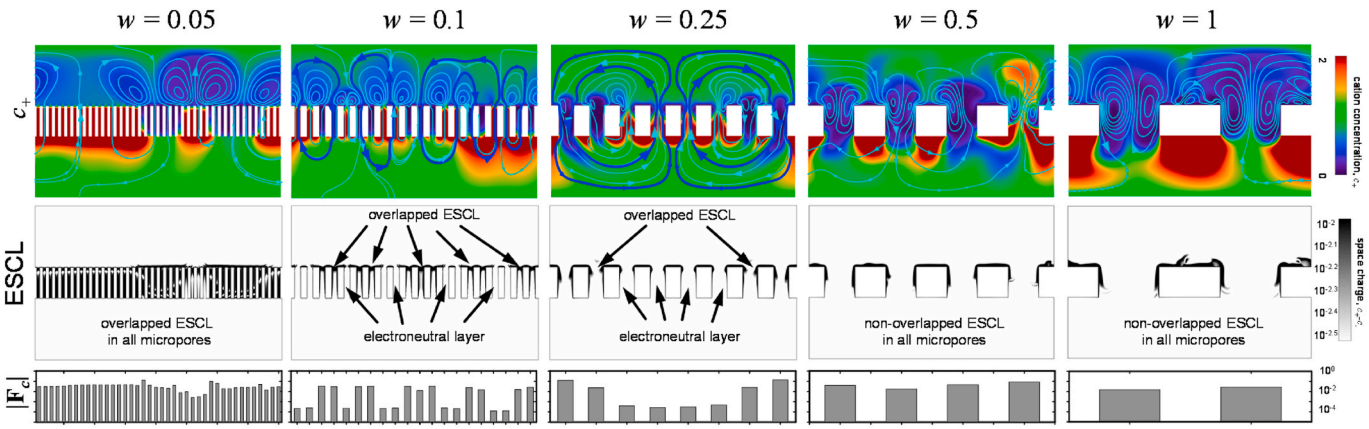

Fig. 4. Numerically simulated concentration profiles/flows streamlines (the first row), the distribution of extended space charge layer (the second row) and the average magnitude of Coulombic force in micropores (the third row) as a function of the width of the micropores; w = 0.05, 0.1, 0.25, 0.5 and 1 in order.

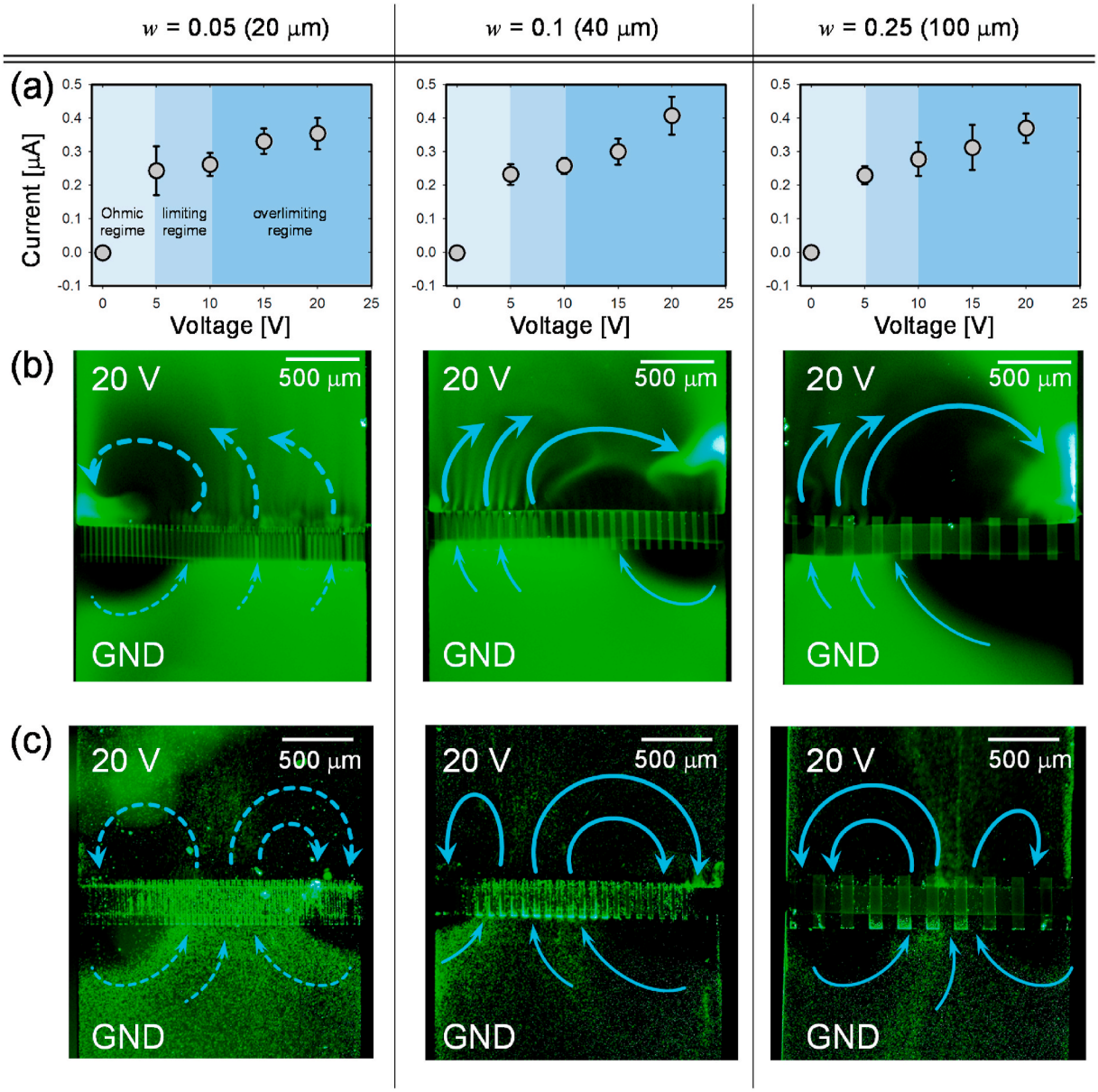

Fig. 5. (a) I–V characteristics of micro/nanofluidic device with multiscale porous membrane. Experimentally obtained (b) concentration profiles using a fluorescent dye and (c) flow profiles using negatively charged particles under 20 V depending on w.

circulating flows were actively formed as indicated in thick blue arrows in the first row of Fig. 4; the direction of circulating flow in the bottom of the electrolyte domain always pointed from the overlapped extended space charge layer regions to non-overlapped regions. See Supplementary Video 4. The presenting system was a closed system that a back pressure must build up and produce a pressure-driven backflow to ensure flow balance. Thus, the circulating flow could be generated by electroconvection and backflow. However, if 1st kind of electroosmotic flow (EOF) and backflow were the main mechanism, the circulating flows should be observed in Ohmic regime as well. It will be discussed later on section 3.5. Therefore, although this system had the 1st kind of EOF and its associated backflow, the main mechanism of circulating flows near multiscale porous membrane should be the electroconvection. As reducing w further (0.05; the first column of Fig. 4), ESCLs in all micropores were overlapped so that there was very small difference in $\mathbf{F_c}$ and the circulating flows were almost vanished. The vortices on the depletion side of the membrane for narrower w resemble the classical electro-convective vortices, because the multiscale porous membrane with much narrower w eventually reaches the conventional nanoporous membrane, which has been extensively studied both experimentally [13,64] and numerically [65]. In addition, the existence of two (or more) vortex states with spatial periodicity that is off by a factor of 2 has recently been reported for the classical case of bifurcated vortices on the depletion side without throughflow [66]. In that paper, different possible steady state of bifurcated vortices was constructed, showing bifurcation branches with spatial periodicity that is off by factors of 2. In the light of their analysis, our study can show a jumping from one bifurcation state to another state intermittently, which is an interesting characteristic of the vortex instability inside ESCL near a permselective membrane.

3.3. Experimental current-voltage relationship for each w

The current-voltage relationship of the concentration polarization platforms showed three distinct regimes called Ohmic regime, limiting regime, and overlimiting regime as shown in Fig. 5(a). In order to analyze the electrical characteristic of the system with multiscale porous membrane, an external voltage ($\widetilde{V}_{app}$) of 5 V, 10 V, 15 V or 20V was applied to the device. After 1 h of applying the voltage, the steady currents at each voltage were obtained by time-average values for an additional hour. The same procedures were repeated at least 3 times for each device using more than 3 devices for the repeatability and reliability. The steady current and voltage response represented Ohmic, limiting and overlimiting regimes as a function of the width of Nafion patch (w) and demonstrated that current behavior above 20 V definitely belonged to the overlimiting regimes in the all w cases. Fig. 5(b) and (c) showed that the concentration and flow profiles were tracked by using fluorescent dye and negatively charged particles, respectively depending on each w.

3.4. Overlimiting current enhancement by electroconvective circulating flow

In order to correlate the circulating flows with the ion transports, numerically and experimentally obtained current densities were compared as shown in Fig. 6. The current density (i) for each w was theoretically calculated by summing the vertical ionic flux divided by the width of the domain and normalized by i_0 which is defined as FDc_0/L in numerical simulation (F is the Faraday constant, D is the diffusivity of ions, c_0 is the bulk concentration and L is the length from upper bulk to an ion-selective patch in the domain of the simulation). In experiments, i was measured at $\widetilde{V}_{app} = 20$ V which belonged to the overlimiting current regime (See Fig. 5(a)) and normalized by $FDc_0/8.2$ mm. The measurements were repeated at least 3 times for each device using more than 3 devices for the repeatability and reliability. The plot presented that the

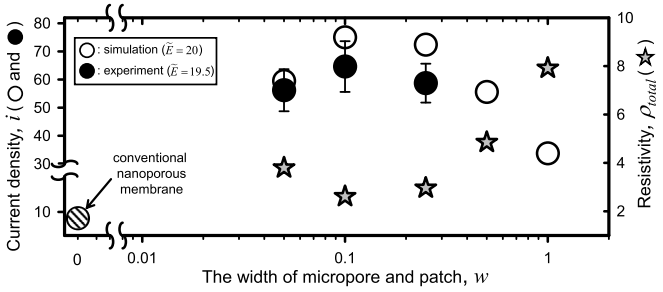

Fig. 6. The plot of the simulated (white circle) and experimental (black circle) current density at an overlimiting regime ($\widetilde{E} = 20$ in numerical simulation and $\widetilde{E} = 19.5$ in experiment). The hatched circle symbols indicated the case of conventional (flat) nanoporous membrane. Star symbols indicated the calculated resistivity of the entire system.

current density had a maximum value at $w = 0.1$ under $\widetilde{E} = 20$ (simulation; white circle) and $\widetilde{E} = 19.5$ (experiment; black circle), which corresponded to the appearance of strong circulating flow depicted in Fig. 4. The current density significantly decreased when $\mathbf{F_c}$s were nearly symmetric, *i.g.* the case of either non-overlapped ESCL in all micropores (*i.e.* $w = 0.5$ and 1) or overlapped ESCL in all micropores (*i.e.* $w = 0.05$). In the case of infinitesimal w which corresponded to a conventional nanoporous membrane without any micropores (hatched circle in Fig. 6), $\mathbf{F_c}$ would be perfectly symmetric (no circulating flow) so that the current density was lower than any other cases. While the experiments were conducted only for the case of $w = 0.05$, 0.1 and 0.25 due to fabrication limits, the results would reasonably reflect this behavior. As stated in 2.2 Experimental methods, the case of $w = 0.5$ and 1 encountered a PDMS collapse in micropores. If the ratio of the width to the height exceeds 10 [61], the microchannel would collapse so that fluid flows through micropores would be blocked or unbalanced. This is why we conducted the simulation to see how the flow field was generated at w values where any experiment was unavailable. For quantitative arguments, we conducted t-test for experimentally measured three current density values. The p value from t-test was 1% between $w = 0.05$ and $w = 0.1$ and 3.5% between $w = 0.1$ and $w = 0.25$, respectively. Thus, all of p values were below 5%, so that it is clear that all of experimental current densities were distinguishable and had the peak at $w = 0.01$.

Note that there was a discrepancy between experimentally and numerically obtained values. This was mainly because the PDMS device has 3D space, while only 2D domain was considered in the simulation for saving computational cost. Also, the device had multiple depths (150 μm in microchannel and 20 μm in micropores) so that this difference would influence potential distribution and fluid flows. However, both results remarkably supported the existence of electroconvective circulating flows increasing the current density and their tendency depending on the patch size.

Since the current density is inversely proportional to the resistivity of the system, we set up an equivalent circuit model to analyze the tendency. A detailed model is described in supplementary note 2. Calculated resistivity (star symbols) from the modeled circuit for each w was plotted in Fig. 6. Replenished ionic carriers due to the formation of cIEZ by the circulating flow would lower total resistivity. Thus, the case of strong circulating flow ($w = 0.1$ and 0.25) possessed the lowest resistivity and the highest current density.

3.5. Electroconvection as the main mechanism of circulating flows

As aforementioned, our system is a closed system so that a back pressure must build up and produce a pressure-driven backflow to ensure flow balance. However, if only 1st kind of EOF and its backflow are considered, the electroconvective circulating flows were not observed and pairs of vortices were trapped between the patches. See

supporting information. Also, it was hard to explain the existence of the maximum current density depending on w (Fig. 6) by considering only 1st kind of EOF and backflow. In addition, the main mechanism of circulating flow would be electroconvection, since the direction of circulating flow in the bottom of the electrolyte domain always pointed from the overlapped extended space charge layer regions to the non-overlapped regions.

Furthermore, if 1st kind of EOF and its associated backflow are the mechanism, the circulating flow should be observed in ohmic regime as well, which is not true. We calculated the absolute value of averaged y-directional velocities inside each micropore (*i.e.* |average(u_y)|, named as "pore velocity"). The value close to zero meant that vortices were trapped inside the micropores, while the value much larger than zero indicated that there was a through flow inside the micropores. We considered the latter case as electroconvective circulating flows near the multiscale porous membrane as shown in Fig. 7(a). Fig. 7(b) showed the contour plot of the average pore velocity depending on w and V_{app}. The plot presented that there was almost no circulating flow under lower V_{app} than 20 (*i.e.* Ohmic or limiting regime) at most of w values, while circulating flows were significant over higher V_{app} than 50 (*i.e.* overlimiting regime) in the case of appropriate w (w = 0.1 or 0.25). These interpretations led to the conclusion that the electroconvective circulating flows were generated in the multiscale porous membrane system with appropriate w in the overlimiting regime. In addition, Fig. 7 (c) showed that the current density had the considerable relationship with the electroconvective circulating flows as similar as Fig. 6. Therefore, it is reasonable to conclude that electroconvection is the mechanism of the circulating flow.

4. Conclusion

In this work, we verified the existence of electroconvective circulating flows near multiscale porous membrane, leading to lowering the resistivity of the entire system and increasing the ion transport. This was demonstrated by a fully-coupled numerical simulation and confirmed by *in situ* visualization and measurement. We found that electroconvective circulating flows were attributed to asymmetric Coulombic forces among the micropores due to an unstable EC. The rigorous analysis of this work revealed the physics behind the questionable current enhancements in previous systems [47,52,53,55]. If one considered an

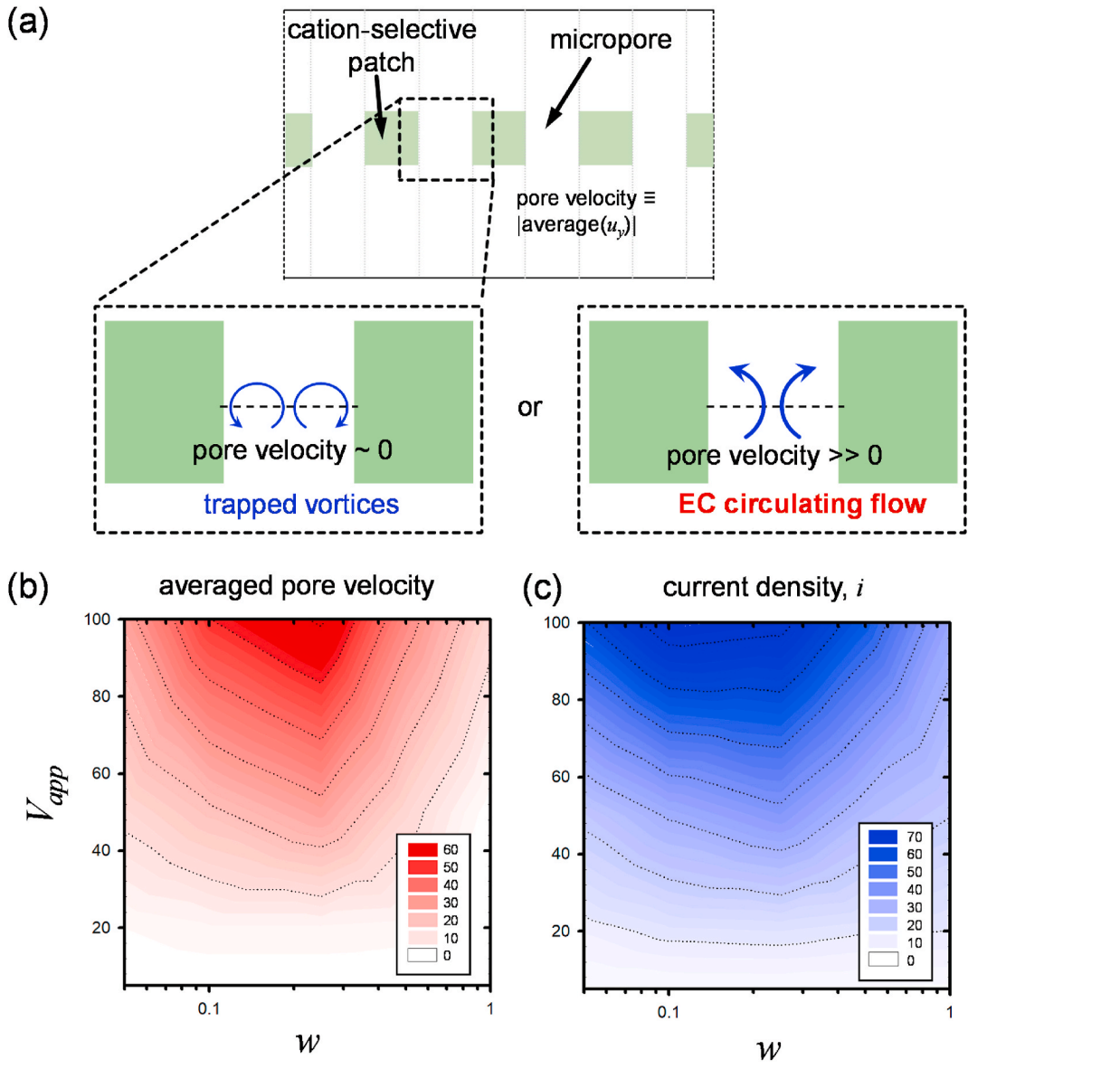

Fig. 7. (a) The schematic diagram of defining "pore velocity". Phase diagrams of (b) averaged pore velocity and (c) its associated current density as a function of V_{app} and w.

external flow to the membrane, which was typical situation in fuel cells or reverse electrodialysis, the circulating flow would still play an important role to determine the current density. See supplementary note 4 for the detailed description. Furthermore, we also revealed that the configuration of ion-selective patches had a critical impact on the current density. In short, the conditions for maximizing ion transport were obtained in the appropriate patch size where abundant circulating flows were evidently formed and decreased the entire resistivity. Conclusively, electroconvective circulating flows near the multiscale porous membrane would provide an effective mechanism for increasing mass transport in various energy-applications that requires high current throughput such as battery or fuel cell, *etc*. and fundamental understandings of electrokinetics near ion conducting spacers.

Authorship contribution statement

Dokeun Lee: Conceptualization, Methodology, Investigation, Writing - original draft.

Daehyun Choi: Investigation.

Hyungmin Park: Methodology.

Hyomin Lee: Conceptualization, Methodology, Writing - review & editing.

Sung Jae Kim: Conceptualization, Methodology, Funding acquisition, Supervision, Project administration, Writing - review & editing.

Declaration of competing interest

The authors declare that they have no known competing financial interests or personal relationships that could have appeared to influence the work reported in this paper.

Acknowledgements

This work is supported by Basic Research Laboratory Project (NRF-2018R1A4A1022513), Mid-Career Project (NRF-2020R1A2C3006162) and Basic Science Research Program (NRF-2020R1C1C1013689) by the Ministry of Science and ICT. In addition, this work is partially supported by BK21 plus program at Seoul National University.

Appendix A. Supplementary data

Supplementary data to this article can be found online at https://doi.org/10.1016/j.memsci.2021.119286.

References

[1] R.B. Schoch, J. Han, P. Renaud, Transport phenomena in nanofluidics, Rev. Mod. Phys. 80 (2008) 839–883.
[2] R.F. Probstein, Physicochemical Hydrodynamics : An Introduction, Wiley-Interscience, 1994.
[3] I. Rubinstein, L. Shtilman, Voltage against current curves of cation exchange membranes, J. Chem. Soc. Faraday Trans. II 75 (1979) 231–246.
[4] I. Rubinstein, F. Maletzki, Electroconvection at an electrically inhomogeneous permselective membrane surface, J. Chem. Soc., Faraday Trans. 87 (1991) 2079–2087.
[5] A. Mani, K.M. Wang, Electroconvection near electrochemical interfaces: experiments, modeling, and computation, Annu. Rev. Fluid Mech. 52 (2020) 509–529.
[6] S.J. Kim, Y.-A. Song, J. Han, Nanofluidic concentration devices for biomolecules utilizing ion concentration polarization: theory, fabrication, and application, Chem. Soc. Rev. 39 (2010) 912–922.
[7] T.A. Zangle, A. Mani, J.G. Santiago, Theory and experiments of concentration polarization and ion focusing at microchannel and nanochannel interfaces, Chem. Soc. Rev. 39 (2010) 1014–1035.
[8] Y. Tanaka, Concentration polarization in ion-exchange membrane electrodialysis: the events arising in an unforced flowing solution in a desalting cell, J. Membr. Sci. 244 (2004) 1–16.
[9] Y. Tanaka, Concentration polarization in ion-exchange membrane electrodialysis—the events arising in a flowing solution in a desalting cell, J. Membr. Sci. 216 (2003) 149–164.
[10] Y. Tanaka, Concentration polarization in ion exchange membrane electrodialysis, J. Membr. Sci. 57 (1991) 217–235.
[11] V.G. Levich, Physico-Chemical Hydrodynamics, Prentice-Hall, London, 1962.
[12] S.J. Kim, Y.-C. Wang, J.H. Lee, H. Jang, J. Han, Concentration polarization and nonlinear electrokinetic flow near nanofluidic channel, Phys. Rev. Lett. 99 (2007), 044501.
[13] S.M. Rubinstein, G. Manukyan, A. Staicu, I. Rubinstein, B. Zaltzman, R.G. H. Lammertink, F. Mugele, M. Wessling, Direct observation of a nonequilibrium electro-osmotic instability, Phys. Rev. Lett. 101 (2008) 236101.
[14] G. Yossifon, P. Mushenheim, Y.C. Chang, H.C. Chang, Nonlinear current-voltage characteristics of nanochannels, Phys. Rev. E 79 (2009).
[15] I. Rubinstein, B. Zaltzman, Extended space charge in concentration polarization, Adv. Colloid Interface Sci. 159 (2010) 117–129.
[16] V.V. Nikonenko, N.D. Pismenskaya, E.I. Belova, P. Sistat, P. Huguet, G. Pourcelly, C. Larchet, Intensive current transfer in membrane systems: modelling, mechanisms and application in electrodialysis, Adv. Colloid Interface Sci. 160 (2010) 101–123.
[17] E.V. Dydek, B. Zaltzman, I. Rubinstein, D.S. Deng, A. Mani, M.Z. Bazant, Overlimiting current in a microchannel, Phys. Rev. Lett. 107 (2011) 118301.
[18] T. Belloň, Z. Slouka, Overlimiting behavior of surface-modified heterogeneous anion-exchange membranes, J. Membr. Sci. (2020) 118291.
[19] T. Belloň, P. Polezhaev, L. Vobecká, M. Svoboda, Z. Slouka, Experimental observation of phenomena developing on ion-exchange systems during current-voltage curve measurement, J. Membr. Sci. 572 (2019) 607–618.
[20] V. Zabolotsky, V. Nikonenko, N. Pismenskaya, E. Laktionov, M.K. Urtenov, H. Strathmann, M. Wessling, G. Koops, Coupled transport phenomena in overlimiting current electrodialysis, Separ. Purif. Technol. 14 (1998) 255–267.
[21] M. Tedesco, H. Hamelers, P. Biesheuvel, Nernst-Planck transport theory for (reverse) electrodialysis: I. Effect of co-ion transport through the membranes, J. Membr. Sci. 510 (2016) 370–381.
[22] A.M. Benneker, B. Gumuscu, E.G. Derckx, R.G. Lammertink, J.C. Eijkel, J.A. Wood, Enhanced ion transport using geometrically structured charge selective interfaces, Lab Chip 18 (2018) 1652–1660.
[23] B. Gumuscu, A.S. Haase, A.M. Benneker, M.A. Hempenius, A. van den Berg, R. G. Lammertink, J.C. Eijkel, Desalination by electrodialysis using a stack of patterned ion-selective hydrogels on a microfluidic device, Adv. Funct. Mater. 26 (2016) 8685–8693.
[24] R. Kwak, V.S. Pham, K.M. Lim, J.Y. Han, Shear flow of an electrically charged fluid by ion concentration polarization: scaling laws for electroconvective vortices, Phys. Rev. Lett. 110 (2013).
[25] K. Nebavskaya, V. Sarapulova, K. Sabbatovskiy, V. Sobolev, N. Pismenskaya, P. Sistat, M. Cretin, V. Nikonenko, Impact of ion exchange membrane surface charge and hydrophobicity on electroconvection at underlimiting and overlimiting currents, J. Membr. Sci. 523 (2017) 36–44.
[26] M.K. Urtenov, A.M. Uzdenova, A.V. Kovalenko, V.V. Nikonenko, N. D. Pismenskaya, V.I. Vasil'eva, P. Sistat, G. Pourcelly, Basic mathematical model of overlimiting transfer enhanced by electroconvection in flow-through electrodialysis membrane cells, J. Membr. Sci. 447 (2013) 190–202.
[27] S.A. Mareev, A.V. Nebavskiy, V.S. Nichka, M.K. Urtenov, V.V. Nikonenko, The nature of two transition times on chronopotentiograms of heterogeneous ion exchange membranes: 2D modelling, J. Membr. Sci. 575 (2019) 179–190.
[28] M. Andreeva, V. Gil, N. Pismenskaya, L. Dammak, N. Kononenko, C. Larchet, D. Grande, V. Nikonenko, Mitigation of membrane scaling in electrodialysis by electroconvection enhancement, pH adjustment and pulsed electric field application, J. Membr. Sci. 549 (2018) 129–140.
[29] L. Alvarado, A. Chen, Electrodeionization: principles, strategies and applications, Electrochim. Acta 132 (2014) 583–597.
[30] L. Alvarado, I.R. Torres, A. Chen, Integration of ion exchange and electrodeionization as a new approach for the continuous treatment of hexavalent chromium wastewater, Separ. Purif. Technol. 105 (2013) 55–62.
[31] K.-E. Bouhidel, A. Lakehal, Influence of voltage and flow rate on electrodeionization (EDI) process efficiency, Desalination 193 (2006) 411–421.
[32] J.-H. Song, K.-H. Yeon, S.-H. Moon, Effect of current density on ionic transport and water dissociation phenomena in a continuous electrodeionization (CEDI), J. Membr. Sci. 291 (2007) 165–171.
[33] J. Choi, S. Baek, H.C. Kim, J.-H. Chae, Y. Koh, S.W. Seo, H. Lee, S.J. Kim, Nanoelectrokinetic selective preconcentration based on ion concentration polarization, BioChip J. (2020) 1–10.
[34] S. Baek, J. Choi, S.Y. Son, J. Kim, S. Hong, H.C. Kim, J.-H. Chae, H. Lee, S.J. Kim, Dynamics of driftless preconcentration using ion concentration polarization leveraged by convection and diffusion, Lab Chip 19 (2019) 3190–3199.
[35] H. Lee, J. Choi, E. Jeong, S. Baek, H.C. Kim, J.-H. Chae, Y. Koh, S.W. Seo, J.-S. Kim, S.J. Kim, dCas9-mediated nanoelectrokinetic direct detection of target gene for liquid biopsy, Nano Lett. 18 (2018) 7642–7650.
[36] L.F. Cheow, J.Y. Han, Continuous signal enhancement for sensitive aptamer affinity probe electrophoresis assay using electrokinetic concentration, Anal. Chem. 83 (2011) 7086–7093.
[37] L.F. Cheow, S.H. Ko, S.J. Kim, K.H. Kang, J. Han, increase of sensitivity of ELISA using multiplexed electrokinetic preconcentrator, Anal. Chem. 82 (2010) 3383–3388.
[38] H. Jeon, H. Lee, K.H. Kang, G. Lim, Ion concentration polarization-based continuous separation device using electrical repulsion in the depletion region, Sci. Rep. 3 (2013).
[39] A. Ciferri, A. Perico, Ionic Interactions in Natural and Synthetic Macromolecules, John Wiley & Sons, 2012.
[40] I. Rubinstein, B. Zaltzman, Electro-osmotic slip of the second kind and instability in concentration polarization at electrodialysis membranes, Math. Model Methods Appl. Sci. 11 (2001) 263–299.

[41] I. Rubinstein, B. Zaltzman, Electro-osmotically induced convection at a permselective membrane, Phys. Rev. E 62 (2000) 2238–2251.
[42] C.L. Druzgalski, M.B. Andersen, A. Mani, Direct numerical simulation of electroconvective instability and hydrodynamic chaos near an ion-selective surface, Phys. Fluids 25 (2013) 110804.
[43] S.M. Davidson, M. Wessling, A. Mani, On the dynamical regimes of pattern-accelerated electroconvection, Sci. Rep. 6 (2016) 22505.
[44] C. Druzgalski, A. Mani, Statistical analysis of electroconvection near an ion-selective membrane in the highly chaotic regime, Phys. Rev. Fluids 1 (2016), 073601.
[45] G. Yossifon, H.C. Chang, Selection of nonequilibrium overlimiting currents: universal depletion layer formation dynamics and vortex instability, Phys. Rev. Lett. 101 (2008) 254501.
[46] J.C. de Valença, R.M. Wagterveld, R.G. Lammertink, P.A. Tsai, Dynamics of microvortices induced by ion concentration polarization, Phys. Rev. E 92 (2015), 031003.
[47] S. Park, R. Kwak, Microscale electrodeionization: in situ concentration profiling and flow visualization, Water Res. 170 (2020) 115310.
[48] A.M. Lopez, J.A. Hestekin, Improved organic acid purification through wafer enhanced electrodeionization utilizing ionic liquids, J. Membr. Sci. 493 (2015) 200–205.
[49] N.A. Shehab, G.L. Amy, B.E. Logan, P.E. Saikaly, Enhanced water desalination efficiency in an air-cathode stacked microbial electrodeionization cell (SMEDIC), J. Membr. Sci. 469 (2014) 364–370.
[50] A. Grabowski, G. Zhang, H. Strathmann, G. Eigenberger, The production of high purity water by continuous electrodeionization with bipolar membranes: influence of the anion-exchange membrane permselectivity, J. Membr. Sci. 281 (2006) 297–306.
[51] C. Huang, T. Xu, Y. Zhang, Y. Xue, G. Chen, Application of electrodialysis to the production of organic acids: state-of-the-art and recent developments, J. Membr. Sci. 288 (2007) 1–12.
[52] H.J. Kwon, B. Kim, G. Lim, J. Han, A multiscale-pore ion exchange membrane for better energy efficiency, J. Mater. Chem. A 6 (2018) 7714–7723.
[53] J. Tang, L. Gong, J. Jiang, Z. Li, J. Han, Numerical simulation of electrokinetic desalination using microporous permselective membranes, Desalination 477 (2020) 114262.
[54] M. Lee, H.J. Kwon, G. Lim, A multiscale-porous anion exchange membrane for convenient and scalable electrokinetic concentration of cationic species, Adv. Funct. Mater. (2020) 2006768.
[55] L. Li, D. Kim, Effect of poly-dispersed nanostructures on concentration polarization phenomena in ion exchange membranes, J. Membr. Sci. 520 (2016) 639–645.
[56] D. Lee, J.A. Lee, H. Lee, S.J. Kim, Spontaneous selective preconcentration leveraged by ion exchange and imbibition through nanoporous medium, Sci. Rep. 9 (2019) 2336.
[57] J.A. Lee, D. Lee, S. Park, H. Lee, S.J. Kim, Non-negligible water-permeance through nanoporous ion exchange medium, Sci. Rep. 8 (2018) 12842.
[58] A.S. Khair, Concentration polarization and second-kind electrokinetic instability at an ion-selective surface admitting normal flow, Phys. Fluids 23 (2011).
[59] J. Choi, A. Mani, H. Lee, S.J. Kim, Investigation on the stability of random vortices in an ion concentration polarization layer with imposed normal fluid flow, Micromachines 11 (2020) 529.
[60] Y. Green, G. Yossifon, Dynamical trapping of colloids at the stagnation points of electro-osmotic vortices of the second kind, Phys. Rev. E 87 (2013).
[61] K. Kim, W. Kim, H. Lee, S.J. Kim, Stabilization of ion concentration polarization layer using micro fin structure for high-throughput applications, Nanoscale 9 (2017) 3466–3475.
[62] S. Ghosal, J.D. Sherwood, H.-C. Chang, Solid-state nanopore hydrodynamics and transport, Biomicrofluidics 13 (2019), 011301.
[63] J. Kim, I. Cho, H. Lee, S.J. Kim, Ion concentration polarization by bifurcated current path, Sci. Rep. 7 (2017) 5091.
[64] G. Yossifon, H.-C. Chang, Selection of nonequilibrium overlimiting currents: universal depletion layer formation dynamics and vortex instability, Phys. Rev. Lett. 101 (2008) 254501.
[65] H.C. Chang, G. Yossifon, E.A. Demekhin, Nanoscale electrokinetics and microvortices: how microhydrodynamics affects nanofluidic ion flux, Annu. Rev. Fluid Mech. 44 (2012) 401–426.
[66] S. Sensale, Z. Ramshani, S. Senapati, H.-C. Chang, Universal features of non-equilibrium ionic currents through perm-selective membranes: gating by charged nanoparticles/macromolecules for robust biosensing applications, J. Phys. Chem. B 125 (2021) 1906–1915.